AD-A169 965   TELESEISMIC WAVEFORM MODELING INCORPORATING THE EFFECTS   1/1
               OF KNOWN THREE-DI   (U) MASSACHUSETTS INST OF TECH
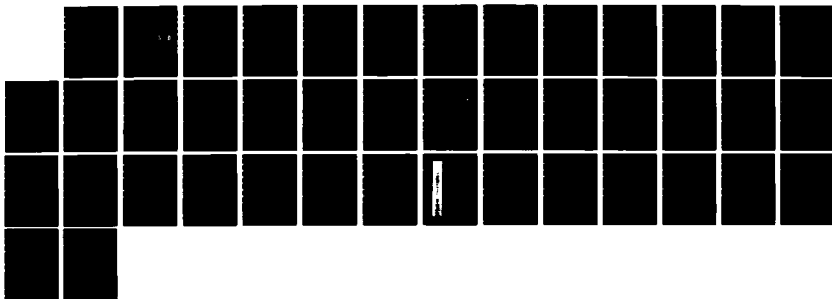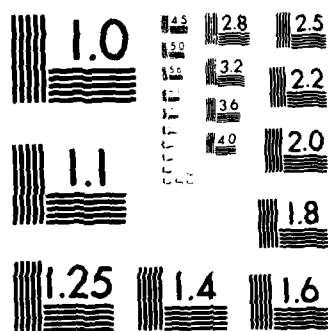   CAMBRIDGE EARTH RESOURCES LAB   V F CORMIER 14 APR 86
UNCLASSIFIED   AFGL-TR-86-0081 F19628-85-K-0031   F/G 8/11   NL

AFGL-TR-86-0081

TELESEISMIC WAVEFORM MODELING INCORPORATING THE
EFFECTS OF KNOWN THREE-DIMENSIONAL STRUCTURE
BENEATH THE NEVADA TEST SITE

Vernon F. Cormier

Massachusetts Institute of Technology
Earth Resources Laboratory
Department of Earth, Atmospheric, and
  Planetary Sciences
Cambridge, MA 02139

14 April 1986

Scientific Report No. 2

APPROVED FOR PUBLIC RELEASE; DISTRIBUTION UNLIMITED

AIR FORCE GEOPHYSICS LABORATORY
AIR FORCE SYSTEMS COMMAND
UNITED STATES AIR FORCE
HANSCOM AIR FORCE BASE, MASSACHUSETTS 01731

REPORT DOCUMENTATION PAGE

1a REPORT SECURITY CLASSIFICATION unclassified	1b RESTRICTIVE MARKINGS
2a SECURITY CLASSIFICATION AUTHORITY	3 DISTRIBUTION/AVAILABILITY OF REPORT
2b. DECLASSIFICATION/DOWNGRADING SCHEDULE	Approved for public release; distribution unlimited

4. PERFORMING ORGANIZATION REPORT NUMBER(S)	5 MONITORING ORGANIZATION REPORT NUMBER(S) AFGL-TR-86-0081

6a. NAME OF PERFORMING ORGANIZATION Earth Resources Laboratory Dept. of Earth, Atmospheric, and Planetary Sciences	6b OFFICE SYMBOL *(If applicable)*	7a NAME OF MONITORING ORGANIZATION Air Force Geophysics Laboratory
6c. ADDRESS *(City, State, and ZIP Code)* Massachusetts Institute of Technology Cambridge, MA 02139		7b ADDRESS *(City, State, and ZIP Code)* Hanscom Air Force Base Massachusetts 01731

8a. NAME OF FUNDING/SPONSORING ORGANIZATION Air Force Geophysics Laboratory	8b OFFICE SYMBOL *(If applicable)* LWH	9 PROCUREMENT INSTRUMENT IDENTIFICATION NUMBER F19628-85-K-0031

8c. ADDRESS *(City, State, and ZIP Code)* Hanscom Air Force Base, Massachusetts 01731 J. Lewkowicz/LWH	10 SOURCE OF FUNDING NUMBERS			
	PROGRAM ELEMENT NO	PROJECT NO	TASK NO	WORK UNIT ACCESSION NO
	61101E	5A10	DA	AJ

11 TITLE *(Include Security Classification)*
Teleseismic Waveform Modeling Incorporating the Effects of Known Three-Dimensional Structure Beneath the Nevada Test Site

12 PERSONAL AUTHOR(S) Vernon F. Cormier

13a TYPE OF REPORT Technical Report No.2	13b TIME COVERED FROM 8/1/85 TO 1/31/86	14 DATE OF REPORT *(Year, Month, Day)* 4/14/86	15 PAGE COUNT 40

16 SUPPLEMENTARY NOTATION

17	COSATI CODES		18 SUBJECT TERMS *(Continue on reverse if necessary and identify by block number)*
FIELD	GROUP	SUB-GROUP	seismic body waves, three-dimensional structure, ray tracing, synthetic seismograms

19 ABSTRACT *(Continue on reverse if necessary and identify by block number)*

Forward calculations have been completed in several models on the effects of three-dimensional structure in the source and receiver site on focussing and defocussing of teleseismic body waves. The choice of models and experiments was designed to separately examine the effects of structure beneath source and receiver sites. Although the models that were examined differed between source and receiver sites, their scale lengths and intensity of velocity fluctuation were similar. This allowed at least a qualitative test of reciprocity of the asymptotic methods used in the forward calculations. The technique used in the forward calculations consisted of body wave synthesis by dynamic ray tracing and Gaussian beams. In experiments that investigated the effects of receiver structure, a plane wave incident on a three-dimensional structure was expanded into Gaussian beams. In experiments that investigated the effects of source structure, the propagator matrix of dynamic ray tracing was employed to connect a 3-D source region to a 1-D whole earth model.

20 DISTRIBUTION AVAILABILITY OF ABSTRACT ☒ UNCLASSIFIED UNLIMITED ☐ SAME AS RPT ☐ DTIC USERS	21 ABSTRACT SECURITY CLASSIFICATION
22a NAME OF RESPONSIBLE INDIVIDUAL James Lewkowicz	22b TELEPHONE *(Include Area Code)*	22c OFFICE SYMBOL AFGL LWH

DD FORM 1473, 84 MAR   83 APR edition may be used until exhausted   SECURITY CLASSIFICATION OF THIS PAGE
All other editions are obsolete

(19. continued)

Calculations were performed in 3-D models of the upper 75 - 100 km. of the crust and mantle beneath the NORSAR array (Thomson and Gubbins, 1982), a model for a region in northern California (Zandt, 1981), and a model generated by random perturbations to a 1-D velocity structure (McLaughlin and Anderson, 1985). In both the NORSAR and Zandt models, azimuthal variations in teleseismic amplitude were found to be on the order of a factor of 2 and variations in travel time were found to be on the order of several 0.1's of a second. These models had a maximum of 4 to 8% velocity fluctuation over scale lengths of 10 to 100 km.

A significant result obtained with the NORSAR and California models was that the scale-lengths and intensities of perturbations were such that the amplitude variations were nearly independent of frequency, and hence adequately predicted by simple ray theory. This result has important consequences for the yield estimation of underground nuclear explosions by measurements of classical body wave magnitudes, m_b, versus broader band measurements of radiated energy in the time and frequency domain. If deep seated, broad scale length (50 km. and greater), velocity anomalies of 2% or more are a common occurrence in the upper mantle of the earth, they will act to focus and defocus body waves over a broad frequency band. The focussing and defocussing caused by these broad anomalies will be independent of frequency and will thus introduce a scatter in broader band measures of radiated energy which will be equivalent to that seen in the narrow band m_b measurement. Focussing and defocussing by structure in the source region will also affect the coda of P waves if a portion of this coda is generated in the receiver again. These effects may help explain why broader band and integrated coda measures of body wave energy often do not exhibit significantly less scatter than classical m_b measurements.

The results obtained with a random model show that a model having a maximum velocity fluctuation as small as 0.8 percent is capable of producing caustics and multipaths at teleseismic range. The production of multipaths strongly depends on the anisotropy of the distribution of scale lengths, i.e., the ratio of characteristic vertical and horizontal scale length. The multipaths of the random model, however, occurred over too small an area and were too closely spaced in arrival time to be resolved with standard seismograph systems operating in the 0.01 to 4 Hz. band.

TELESEISMIC WAVEFORM MODELING INCORPORATING THE EFFECTS OF KNOWN

THREE-DIMENSIONAL STRUCTURE BENEATH THE NEVADA TEST SITE

Scientific Report No. 2

Period Reported: 1 August 1985 to 31 January 1986

14 April 1986

Sponsored by:

Principal Investigator

Dr. Vernon F. Cormier

(617) 253-7862

1 Introduction

The 3-D structure beneath source and receiver can act to focus and defocus teleseismic body waves. In the receiver region, the focussing and defocussing may account for variations in m_b over a 200 km aperture array as large as that seen over an array having teleseismic dimensions. The following sections summarize results of forward modeling experiments designed to measure the amplitude fluctuations predicted by known 3-D structure beneath sources and receivers obtained by block 3-D inversion of travel times. The importance of such models is that they can always be obtained for a particular test site given known source locations and times within a test site, supplemented by constraints on local crustal structure. Given such models and the location of an event within a test site, it is possible to calculate a magnitude bias factor, which can be used to correct for the focussing/defocussing effects of the structure. This factor would vary as a function of event location within the test site and azimuth of the receiver station. Similarly, corrections for the effects of structure beneath receiver arrays may be formulated.

This report details the results of the first complete year of research on problems of focussing and defocussing. Several source and receiver models have been investigated in addition to a model of NTS by Minster *et al* (1981). The scale lengths of this NTS model were too broad and the intensity of velocity fluctuation was too week to produce any significant amplitude fluctuations. Next a sequence of models having stronger velocity fluctuations were investigated in order to determine the resolution needed to predict significant focussing/defocussing effects. Thus far, these include a model beneath NORSAR, a model of the crust and uppermost mantle beneath northern California, and a random model constructed to satisfy the characteristic statistics of magnitude variations. The results reported for the NORSAR model were calculated by Robert Nowack while he was post-doctoral fellow at M.I.T., supported by this contract The experiments with the Zandt and random models have been submitted for

publication in GJRAS (Cormier, 1986). A paper on the NORSAR results is in preparation by Nowack and Cormier.

2 Receiver structure: the NORSAR model

2.1 DESCRIPTION OF MODEL

The structure beneath NORSAR has been studied by a number of investigators using teleseismic travel time data. In the examples shown here, the model derived by Thomson and Gubbins (1982) is used. This velocity model is a variation of the model originally derived by Aki *et al.* (1976), which was the first application of seismic travel time inversion for a 3-D structure.

Good quality amplitude data has been recorded at NORSAR and has been studied by several investigators. Haddon and Husebye (1978) used a thin lens model at a depth of 150 to 200 km to describe both the amplitude and travel time data. Statistical models for amplitude fluctuations at NORSAR were investigated by Berteussen (1975) and Berteussen *et al* (1975). Thomson and Gubbins (1982) compared the amplitude data to that predicted by the travel time models and found only moderately good agreement, with the predictions not showing large enough variations across the array. Thomson (1983) attempted a separate inversion of the amplitude data with again only a moderately good agreement with the travel time inversion results. Thomson (1983) suggested the possibility that ray theory may not give reasonable predictions of the amplitude data for frequencies of 1.0 to 3.0 Hz, for a structure such as NORSAR.

Recently an amplitude comparison was done by Haines and Thomson (1986) between the Phase Front method developed by Haines (1983) and the ray amplitudes computed using the ray bending method. Their comparison showed quite different results between the two methods and their interpretation was that ray theory did allow for the finite frequency effects. This is a very interesting result since the NORSAR

velocity model is smoothly varying with length scales on the order of 20. km., which approach the wavelengths of short period body waves. We were then interested in comparing amplitudes derived from ray theory with Gaussian beam amplitudes using this NORSAR velocity model. C. Thomson provided us with velocity model A2 from Thomson and Gubbins (1982) for this comparison.

Figure 1 shows this velocity model for NORSAR. The model is 180. km in depth. The spheres in Figure 1 represent lower velocities and the cubes represent higher velocities. Only velocity fluctuations greater than 3.5% are shown, with the size of the symbol corresponding to the magnitude of the velocity fluctuation from the average vertical velocity structure. The east side of the model, with values of x greater than 45. km, is in general fast and the west side of the model is slow. The largest fluctuations are $\pm$ 8% and occur in the deepest layer from 96. to 120. km.

In order to display the velocity model more clearly, Figure 2 shows the variations greater than 1.5% for each layer. Layer 1 is similar to Layer 2 with smaller relative velocity fluctuations and is not shown. Layer 2 is from 24. to 48. km and has higher velocities in the south-central regions. The Oslo Graben intersects this region from the south and trends in a NNE direction. The NORSAR Array occupies the middle 100. km on the surface of the model region. Layer 3 is from 48. to 72. km, and the higher velocities have now shifted to the east. Layer 4 is from 72. to 96. km. The velocity fluctuations are larger with lower velocities in the south and west and higher velocities to the east. Finally, the deepest layer, Layer 5, goes from 96. to 120. km, the inferred depth of the lithosphere. The largest fluctuations are seen to occur in this layer with high velocities to the east and a U-shaped region of lower velocities to the south and west. It is interesting to consider why the derived velocity fluctuations increase with depth, since the resolution of the derived solution of these lower layers appears to be adequate. One might intuitively think that the shallow layers should be more heterogeneous and therefore have a greater intensity of velocity fluctuation. Since significant velocity perturbations continue into the deepest layer of this model, it suggests that less
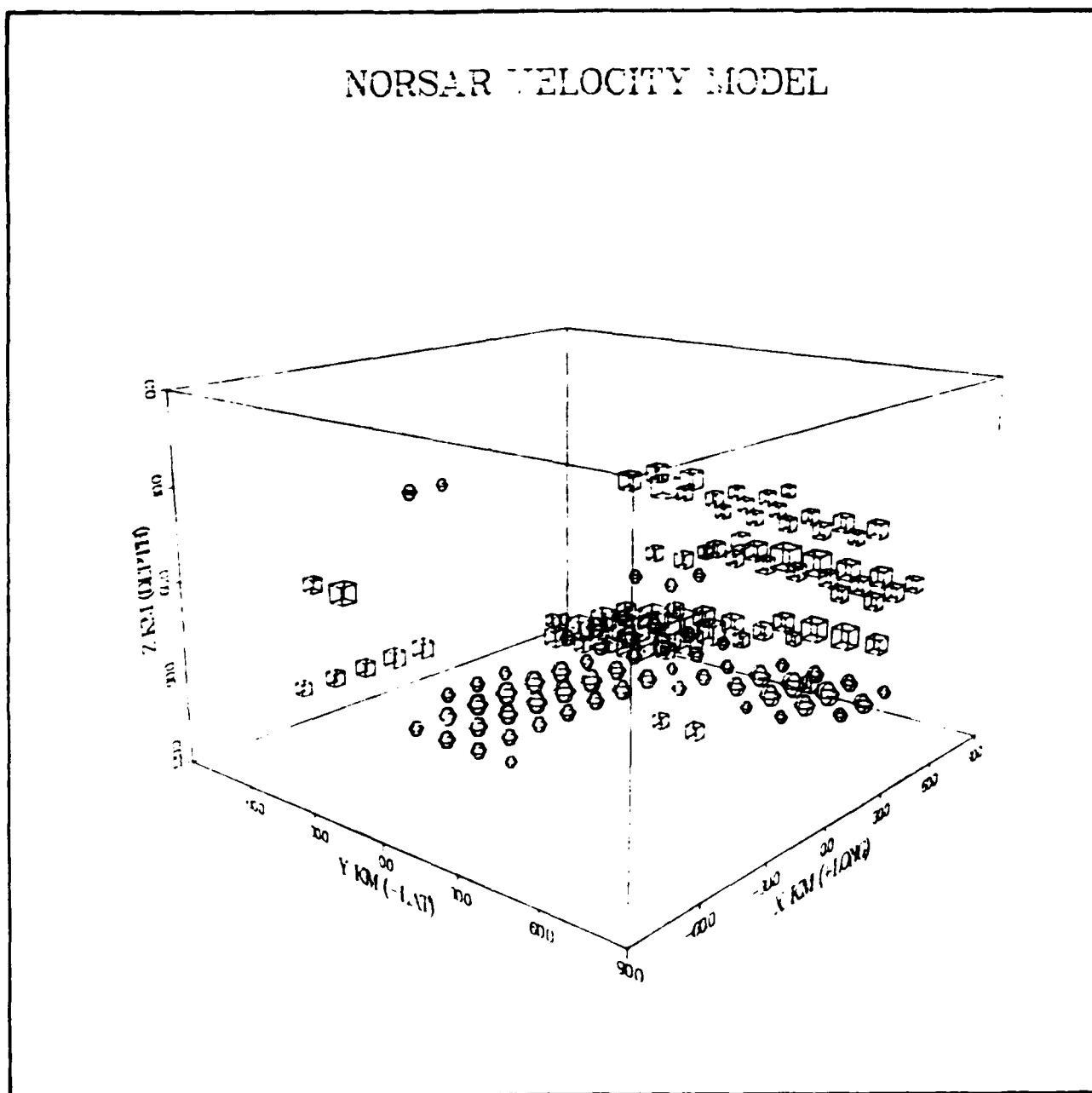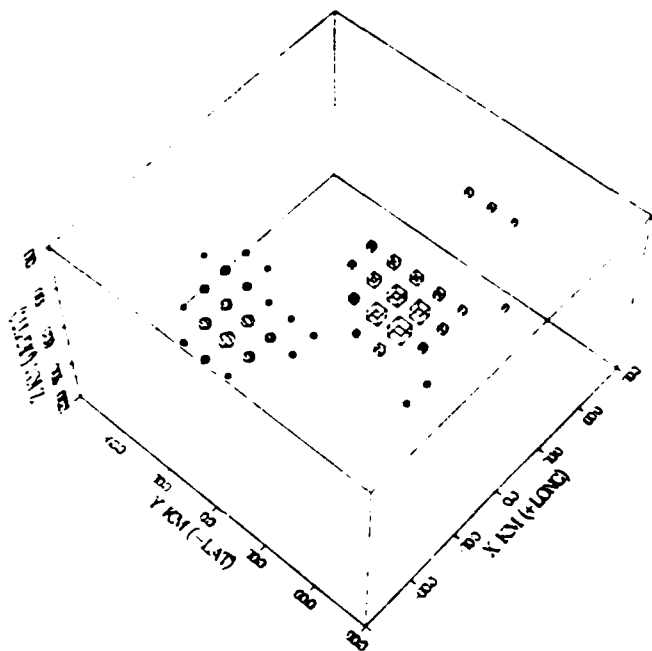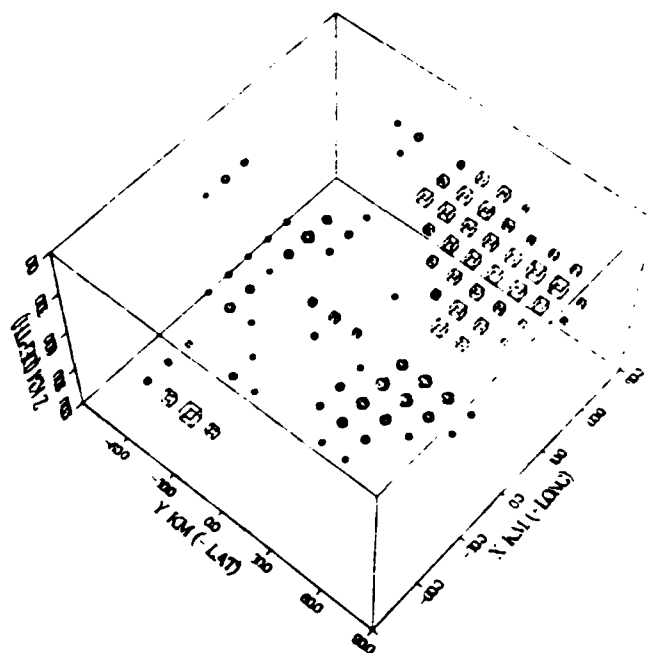
Figure 1. Velocity model of NORSAR by Thomson and Gubbins (1982). Variations greater than 3.5% are shown.

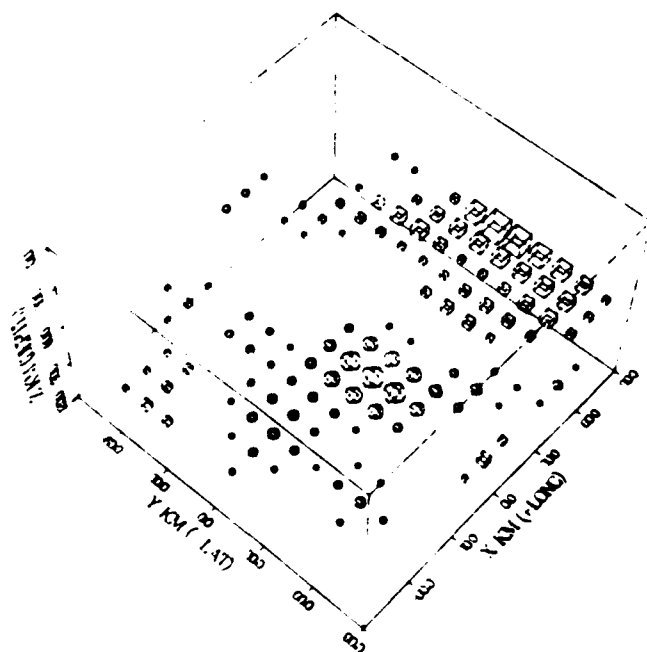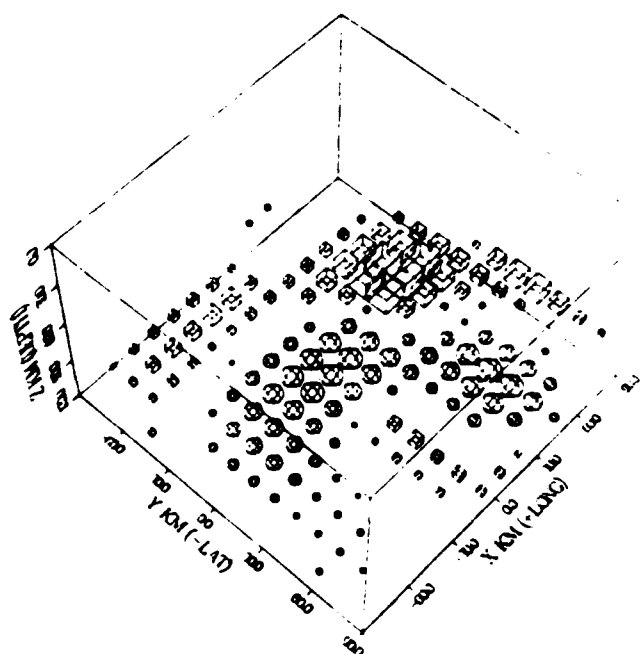Figure 2. Velocity model of NORSAR. Variations greater than 1.5% are shown.

intense perturbations that continue below the model may have been mapped by the inversion into the lowest layers of the model.

2.2 COMPARISON WITH THE PHASE FRONT METHOD AND RAY THEORY

Figure 3 shows the location of the NORSAR Array and three specific events, with distances from 57° to 70°, used by Haines and Thomson (1986). To compare with their results, ray amplitudes using the shooting method were computed. To do this, rapid two-point ray tracing was required and here the paraxial ray equations were used to find the boundary value rays (Červený *et al*, 1984).

Figure 4 shows an example of this where the ray from A to B is given and we want to use the paraxial ray equations to determine the ray from A_1 to B_1. Since this is only an approximation, iteration is required to find the exact ray. The problem investigated here is a slight variation of this where an initial wavefront is given with some initial ray directions, and the ray eminating from the wavefront surface going to a particular station is required. Using the iterative application of the paraxial ray equations, excellent convergence properties were found. Typically only two or three iterations were required to get within .1 km of the station using the NORSAR velocity model.

Figure 5 shows the rays going through the NORSAR model from teleseismic events A, B, and C in Figure 3. Twenty-five equally spaced stations were specified on the surface covering the general location of the NORSAR array. The ray trajectories were checked at each point along the ray by using the eikonal equation. The paraxial ray equations were then used once again to compute the amplitudes at the stations. Our derived amplitudes were checked with ray differencing calculations and the comparisons were within 1 percent.

Our computed ray amplitudes were then compared with the results of Haines and Thomson (1986). In comparing the ray bending amplitude calculations to our ray calculations, there were some discrepancies at particular points Part of this
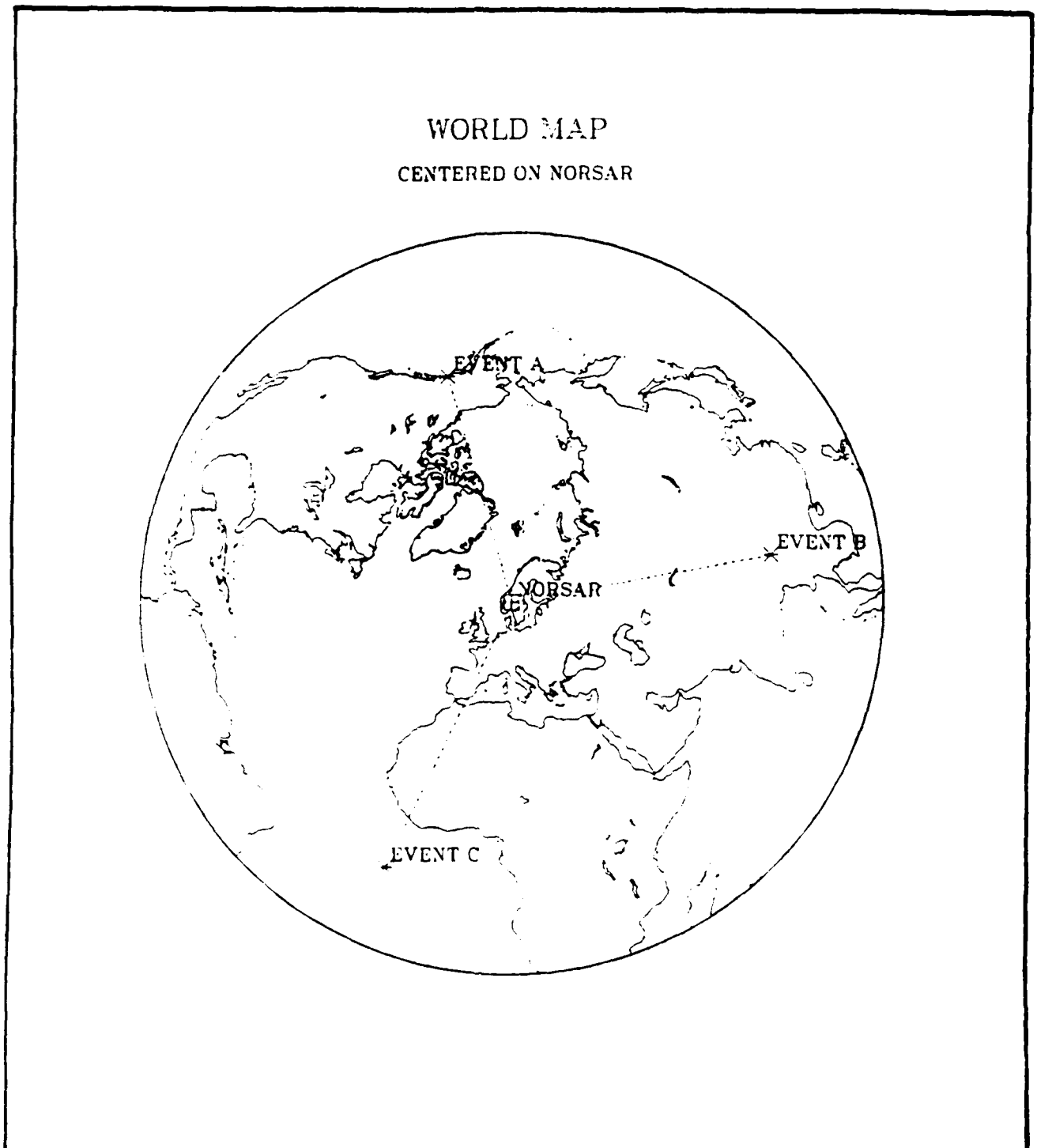
Figure 3. Location of NORSAR array and three events studied by Haines and Thomson (1986).

Boundary Value Ray Tracing

Application of paraxial ray equations
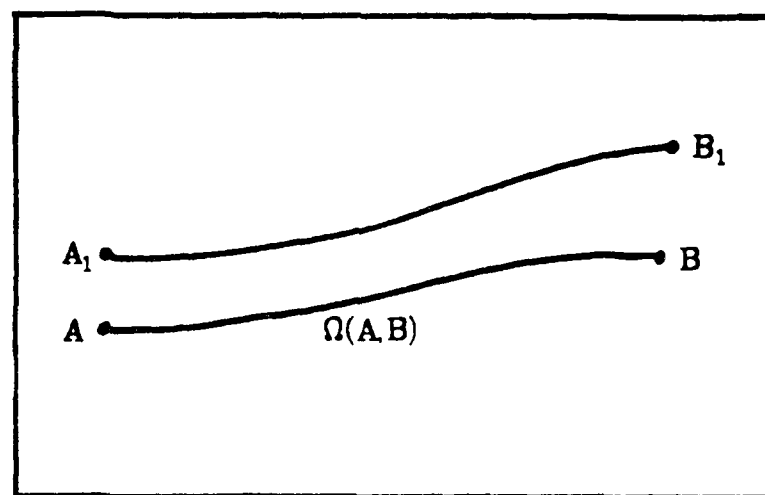
Given the ray $\Omega(A,B)$, find the approximate ray $\Omega(A_1,B_1)$.

Application: the calculation of a normal ray

from an initial wavefront.

Figure 4. Paraxial approximations can be used to develop an iterative scheme to solve the two point ray tracing problem. These approximations are valid in the neighborhood of ray AB and can be used to find a ray $A_1 B_1$ that solves a two point ray tracing problem.

PARAXIAL BOUNDARY VALUE RAY TRACING
EVENT A
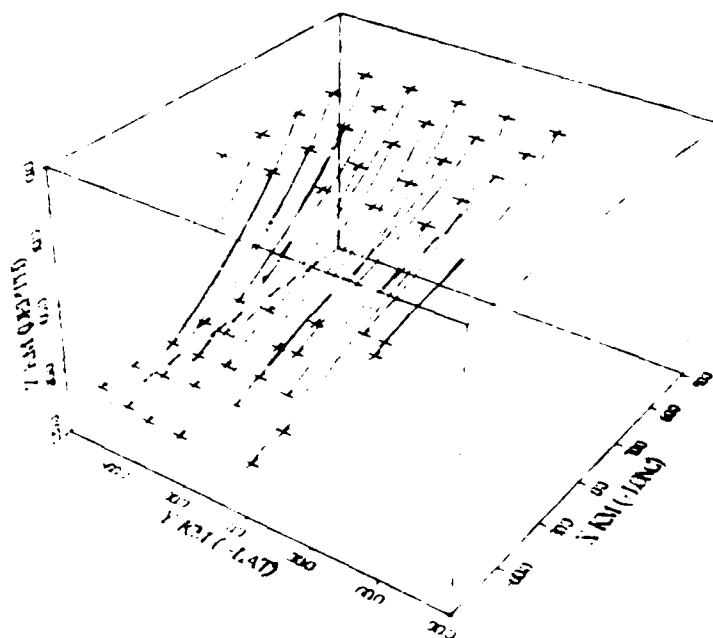
PARAXIAL BOUNDARY VALUE RAY TRACING
EVENT C
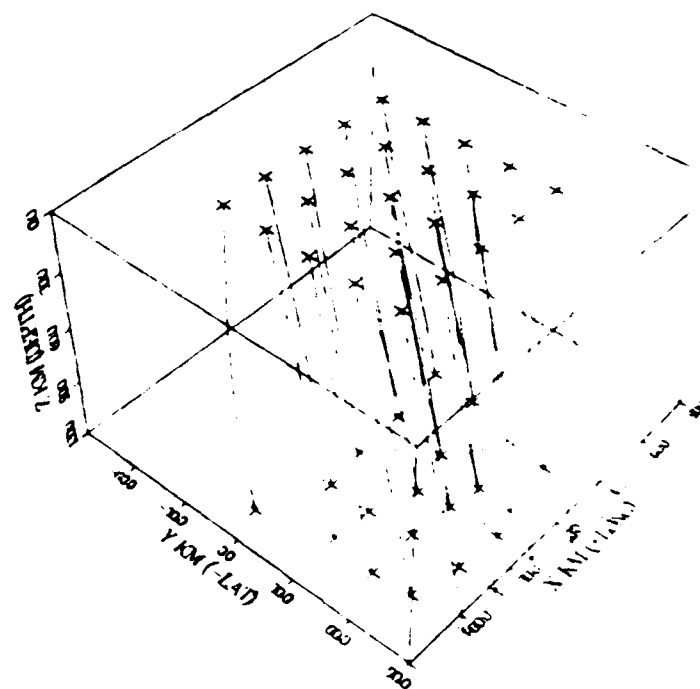
PARAXIAL BOUNDARY VALUE RAY TRACING
EVENT B

Figure 5. The rays from the NORSAR model from the teleseismic events A, B,
and C of Figure 3.

discrepancy involved boundary value rays, shown in Figure 5, that exit the model on the sides of the box. Our ray amplitudes resulted from extending the box by 100. km on all sides. It is unclear how the ray bending calculations handled this. These particular events had distances between 57° to 70°. For the actual data, distances of the events ranged from 25° to over 100°, and for the closer events this problem of rays exiting from the sides would increase.
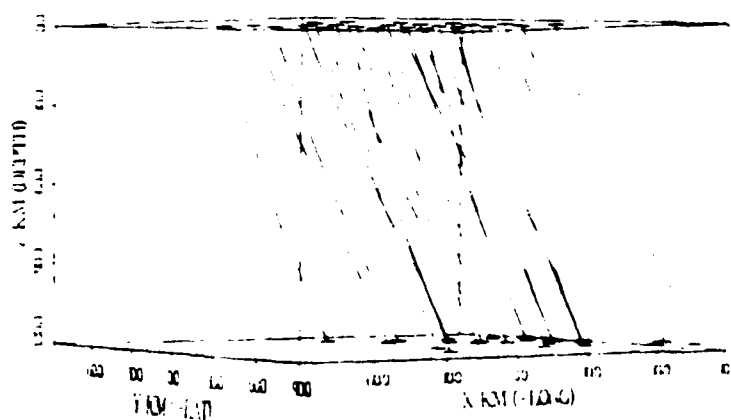
Excluding the stations which had rays that exited the model from the sides, only four points for the three events A, B, and C varied by more than 15% in amplitude from the ray bending calculations of Haines and Thomson (1986). The remaining differences are assumed to be from slight parameterization differences of the model. With these considerations, the Phase Front calculations of Haines and Thomson (1986) were not in agreement with either the ray bending calculations or our paraxial ray calculations. Also the differences of the Phase Front calculations with frequency an the ray calculations did not vary in a systematic fashion. Since both the Phase Front and Gaussian beam methods involve similar parabolic approximations, the expectation was that they should have been in excellent agreement. Haines and Thomson note that the Gaussian beam method would be inaccurate in the deep shadow of a caustic compared to the Phase Front method. The NORSAR model, however, generated no caustics over the short ray paths of the expanded plane wave. With these considerations, our preliminary conclusion is that there may be some errors in Haines and Thomson's application of the phase front method.

2.3 FREQUENCY DEPENDENCE

In the following, a comparison was done between ray theoretical amplitudes and Gaussian beam amplitude for several frequencies. To simplify the comparison, a vertically incident plane wave from below the NORSAR model was used. Figure 6 shows the variation of travel time at the surface of the model for the vertically incident plane
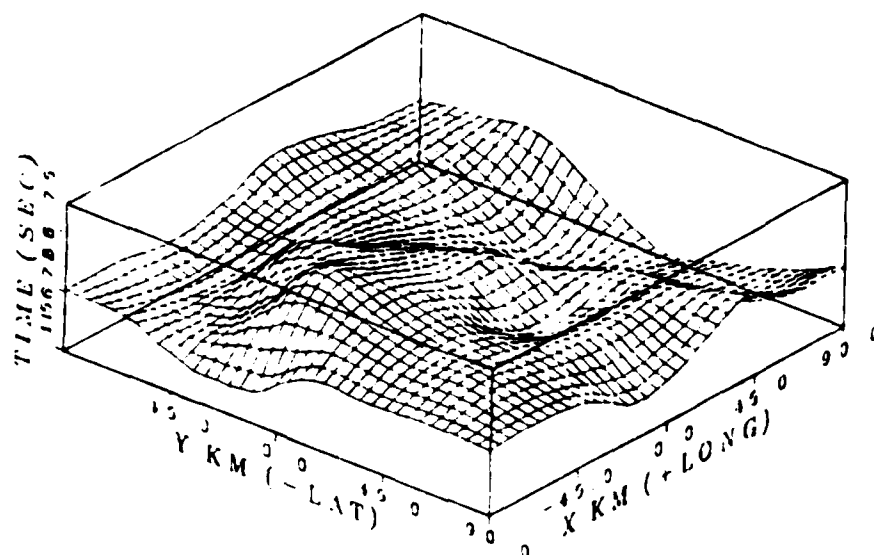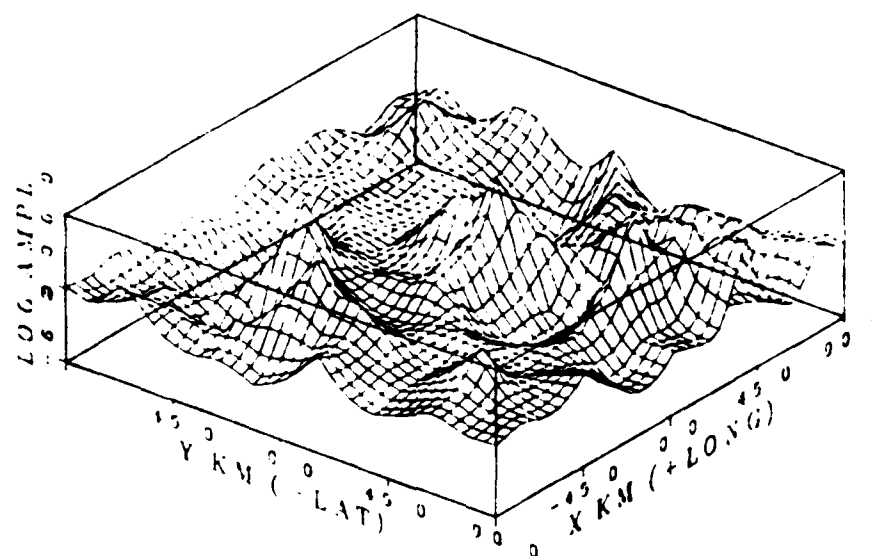
TRAVEL TIME VARIATIONS

LOG AMPLITUDE VARIATIONS
## PARAXIAL RAY THEORY

Figure 6. Variations in travel time and amplitude for a plane wave incident on the NORSAR model.

wave from below. The time scale is 1.0 sec. Comparing with the velocity model in Figure 2, the delayed times of the travel time surface are associated with the slower U shaped velocity region in the lowest layer of the model to the south and west. The earlier times to the southeast are associated with faster velocities. The corresponding amplitude surface for this case is also shown in Figure 6. The amplitude values plotted in 20. Log (A/S_0), are shown with a vertical scale going from -6.0 to +6.0 db. The amplitude surface can be seen to be much rougher than the travel time surface. This is consistent since the log amplitudes are proportional to $\nabla^2 T$ integrated along the path. The higher amplitudes are seen to be associated with the delayed travel times.

Next, the smaller central region of the model covered by the NORSAR seismic array was investigated. The amplitudes, in db, for this smaller region are shown in Figure 7. The vertical scales go from -5. to +5. db. Berteussen (1975) found at NORSAR a range of amplitudes of 14. db. The variation shown here is about .6 db for this vertically incident case. The paraxial ray amplitude surface shown in Figure 7 has a high peak to the northwest, a central high amplitude region with a lower amplitude to the south, and a gradual increase in amplitude to the southeast.

The Gaussian beam results were computed using a simple Gabor wavelet with a $\gamma =$ 6. and several center frequencies. Optimal or critical beam widths are specified at the source plane (Červený, 1982, 1985a, 1985b, and Klimes, 1984). The peak amplitudes are then plotted. The 8. Hz Gaussian beam result is shown in Figure 7, and all the features shown in the ray amplitude diagrams are present. But, the two high amplitude regions are slightly lower in amplitude than the corresponding ray results. The 4. Hz Gaussian beam result shown in Figure 7 is very similar except the amplitude peak to the northwest is slightly lower still. Finally, the 1.0 Hz Gaussian beam case is shown and now the amplitude peak to the northwest is rounded and broadened and the whole amplitude surface has been smoothed. Thus, there appears to be a progression from the ray amplitude results to the high frequency beam results, with greater similarity for higher frequencies. The frequency dependence between 1 to 8 Hz, however, is small.
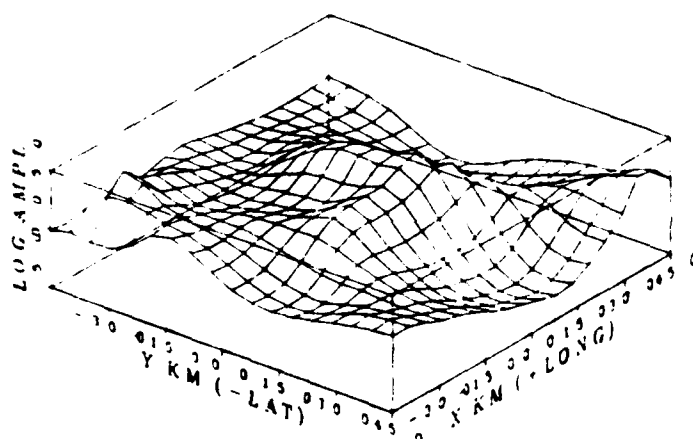
LOG AMPLITUDE VARIATIONS
PARAXIAL RAY THEORY
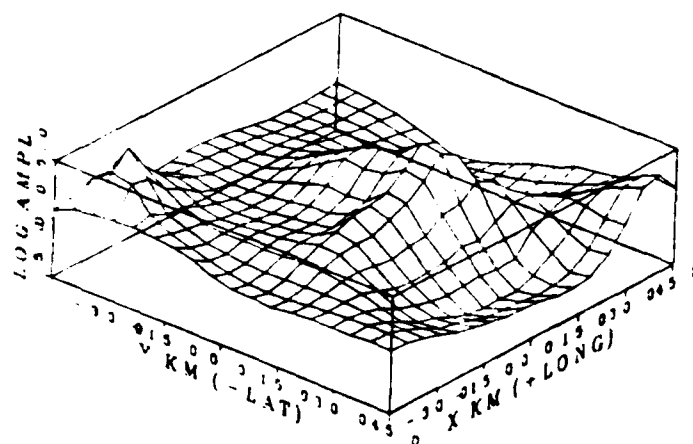
LOG AMPLITUDE VARIATIONS
GAUSSIAN BEAM – 8 HZ
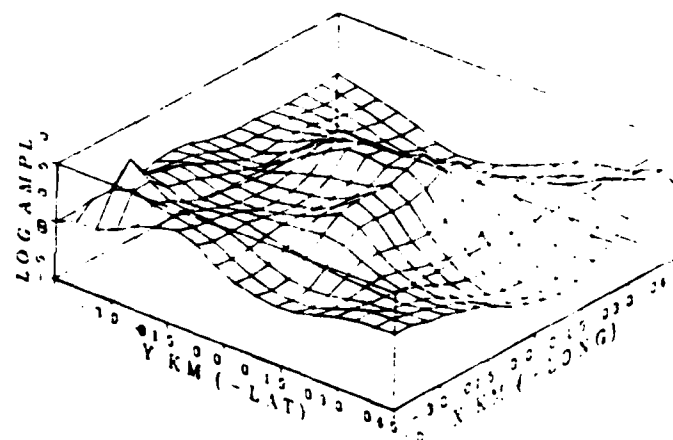
LOG AMPLITUDE VARIATIONS
GAUSSIAN BEAM – 4 HZ
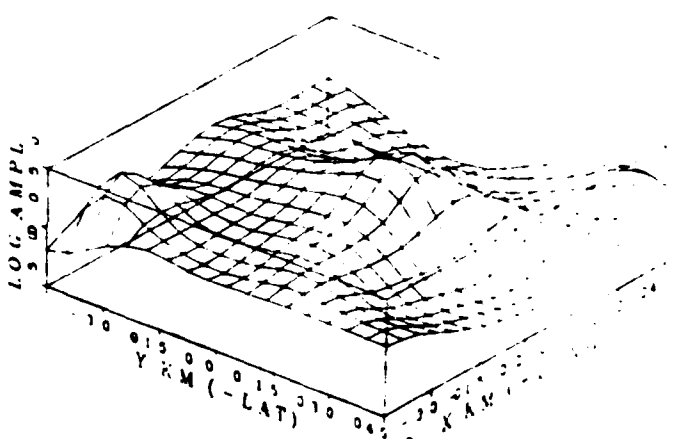
LOG AMPLITUDE VARIATIONS
GAUSSIAN BEAM – 1 HZ

Figure 7. Variations in amplitude for a vertically incident plane wave on the NORSAR model. Results for several frequencies are shown.

This is consistent with the scale lengths of this model, which are broad (20 km.) compared to the wavelengths at these frequencies (greater than 8 km.). Since the wavelengths for the 1., 4. and 8. Hz cases are 8., 2., and 1. km with approximate Fresnel zone radii of 20., 12., and 8. km. the Gaussian beam solutions should give reasonable results for the NORSAR model, at least down to 1. Hz.

In summary, the beam amplitude results behave in a similar fashion to the ray amplitude results with the lower frequency beam solutions becoming smoother. This suggests the possibility of using lower frequency amplitude data to smooth over unwanted amplitude variability to obtain results for an equivalent smooth median. The paraxial ray equations have been used for the 2-point boundary value ray calculation and have shown very rapid convergence.

3 Source structure

3.1 THE NORTHERN CALIFORNIA MODEL

The focussing and defocussing of teleseismic body waves by 3-D structure in the vicinity of the source have been investigated with two different models. The first model is one obtained by Zandt (1981) for central California using a block inversion of teleseismic travel times by the method of Aki et al (1976).

The Zandt (1981) model has four layers from 0.0 to 90.0 km in depth. The horizontal block size is 10.0 km in the top layer and 20.0 to 25.0 km in the lower layers. Average velocity variations are between 4.0 to 8.0 percent in the top layer and 2.0 to 1.0 percent in the lower layers. The rms velocity variation measured over grid points, however, is generally much lower, on the order of less than 2 percent. This is because the largest variations take place over relatively broad regions, having characteristic scale lengths of between 50 to 100 km. (Figure 8)
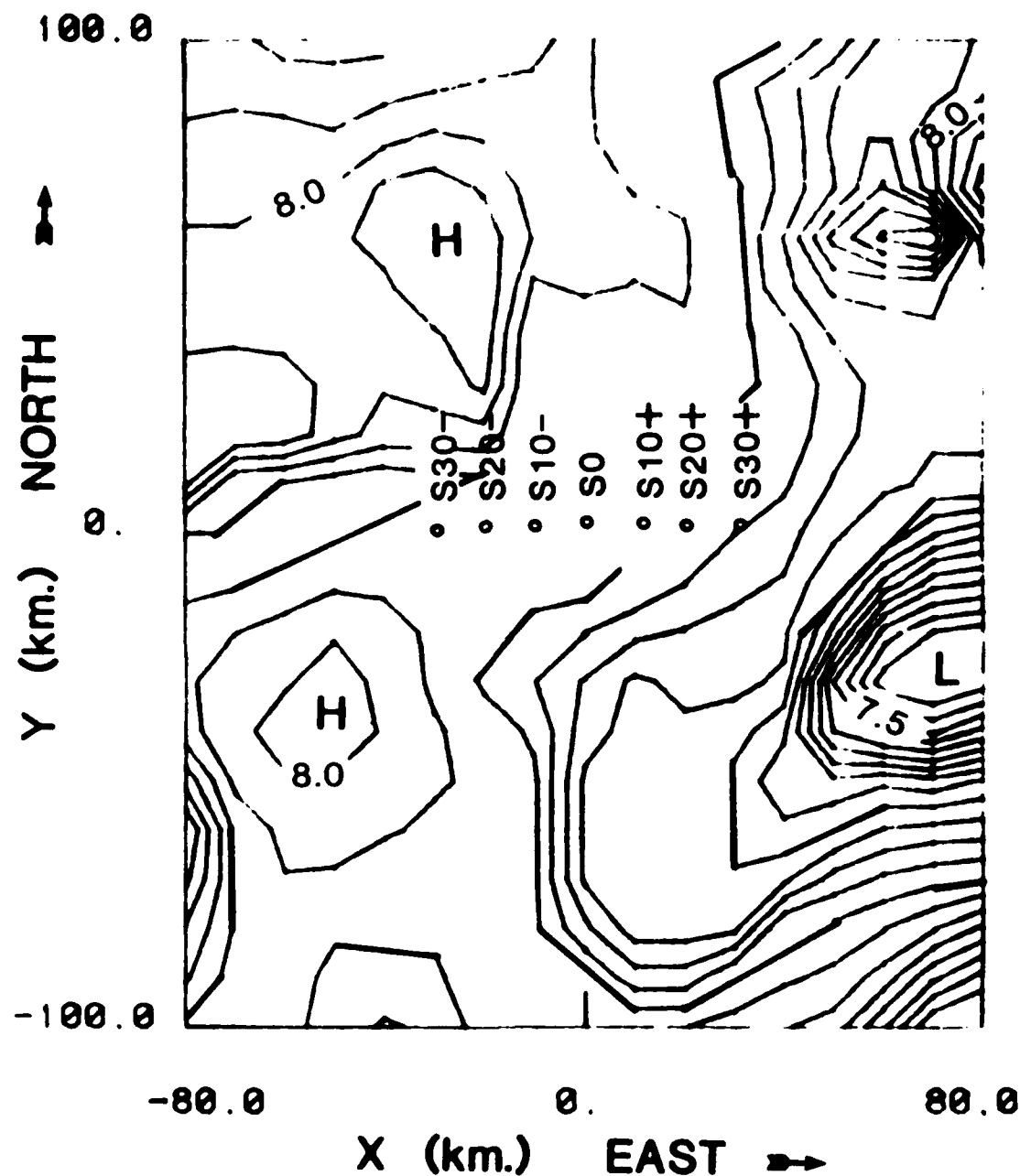
Figure 8. P velocity contours in a horizontal plane at 90 km. depth in the 3-D model for central California by Zandt (1981). Also shown are the projections of source locations used in propagation experiments at teleseismic range.

Seismograms were synthesized in this model by summation of Gaussian beams. An explosive point source was assumed at the center of the model at 9.6 km depth. The 3-D model was patched into a 1-D, flattened whole earth model by use of the propagator matrix of dynamic ray tracing (Cormier, 1986). The elements of the propagator matrix Π were calculated in the 3-D source region by numerical integration of the kinematic and dynamic ray tracing equations. Velocities and their first and second order spatial derivatives in the 3-D region were defined by the coefficients of cubic spline interpolators between grid points. The 3-D region was patched into a 1-D, radially symmetric earth model at 75 km depth. The 1-D earth model was the 1 Hz., isotropic PREM of Dziewonski and Anderson (1981). PREM was first flattened using the transformations described by Müller (1971). The Π elements were then computed using a fast algorithm in which the quantities $\frac{dX}{dp}$ and X are given by a analytic formulae summed over thick, vertically inhomogeneous layers (Červený and Janský, 1983). Π was determined at the ray end points in the receiver region by propagator multiplication. The matrices P^R, Q^R needed to evaluate the weighting factor for superposition of Gaussian beams are given by the 2 x 2 sub-matrices of Π, Π_{22} and Π_{12} respectively. Focussing/defocussing effects of the structure were calculated at teleseismic range for the variations in azimuth and variations in lateral source location shown in Figure 8.

3.1.1 Effect of varying azimuth at constant source location

Figure 9 shows the results of beam summation for a teleseismic P wave from an explosive source embedded in the Zandt (1981) model. At source location s0, seismograms were computed at 70° for eight different azimuths. In each column of Figure 9, the amplitudes predicted in different pass bands are shown. The broadband pulse was that obtained using the source-time function of Madariaga and Papadimitriou (1985) in a frequency band between 0.03 to 4 Hz. Amplitudes are scaled to the maximum peak to peak amplitude observed at the 101° azimuth. Amplitude variations
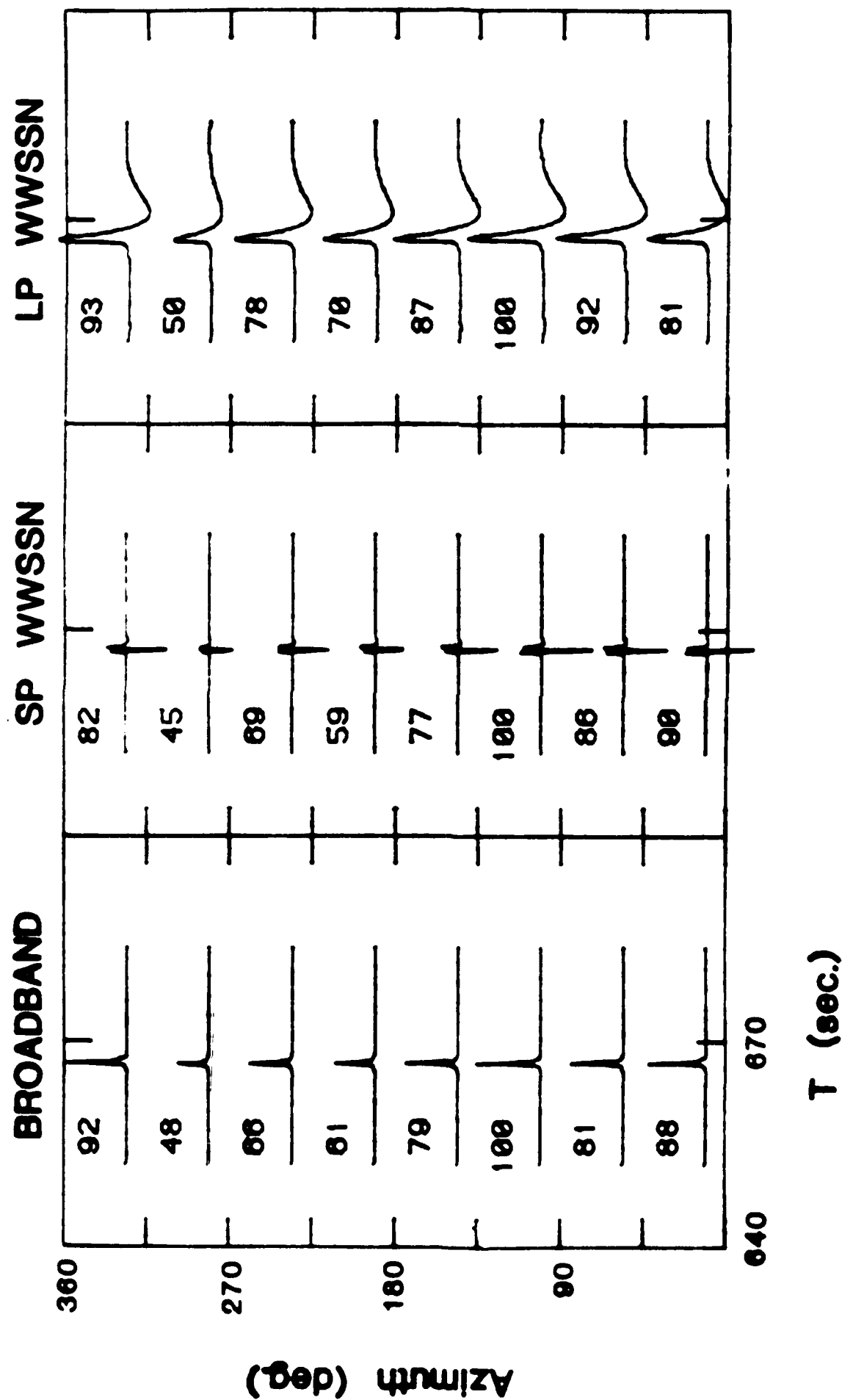
Figure 9. Synthetic seismograms constructed by superposition of Gaussian beams for stations at 70° and variable azimuths from an explosive point source at a constant location S0 at 9.6 km depth in the Zandt model. Seismograms are shown for a broad band, WWSSN short period and long period instrument response.

18.

are on the order of two and travel time variations on the order of several 0.1's of a
second. The travel time variations are consistent with the focussing/defocussing
effects -- large amplitudes correlate with slow travel times and small amplitudes
correlate with fast travel times. The largest amplitudes correlate with azimuths in
which the beams sample a low velocity anomaly to the southeast of source s0. This
anomaly is a significant feature in both layers 3 and 4 of the Zandt model, persisting
over 50 km of depth in the model. Zandt interprets this feature as a NW-SE trend of
lithospheric thining associated with a fault zone that includes the Calaveras, Rogers
Creek, Maacama, and Lake Mountain faults.

3.1.2 Effect of varying source location at constant azimuth

For a fixed azimuth, and variations in source site from positions s30- to s30+
(Figure 10), amplitude variations are small. This reflects the smaller differences in
structure between the regions sampled by the beams compared to those in the
azimuthal experiment. The velocity anomalies in the deeper layers are broad features
having scale lengths of 50 km or more. The anomalies in the shallower, crustal layers
have smaller scale lengths, but the crustal layers are thin compared to the total
thickness of the model and the beams spend much longer time in the thick layers 3 and
4. Thus the broad scale lengths of the anomalies in layers 3 and 4 have the greatest
influence on amplitudes. This is consistent with the large variations in amplitude shown
in the azimuthal experiment (Figure 9) as well as with the smaller variations in
amplitude due to changes in receiver location over a line having a length roughly equal
to the scale length of the broad anomalies (Figure 10).

3.1.3 Frequency independence and its implications for treaty verification

The relative amplitudes in Figures 9 and 10 are nearly independent with respect to
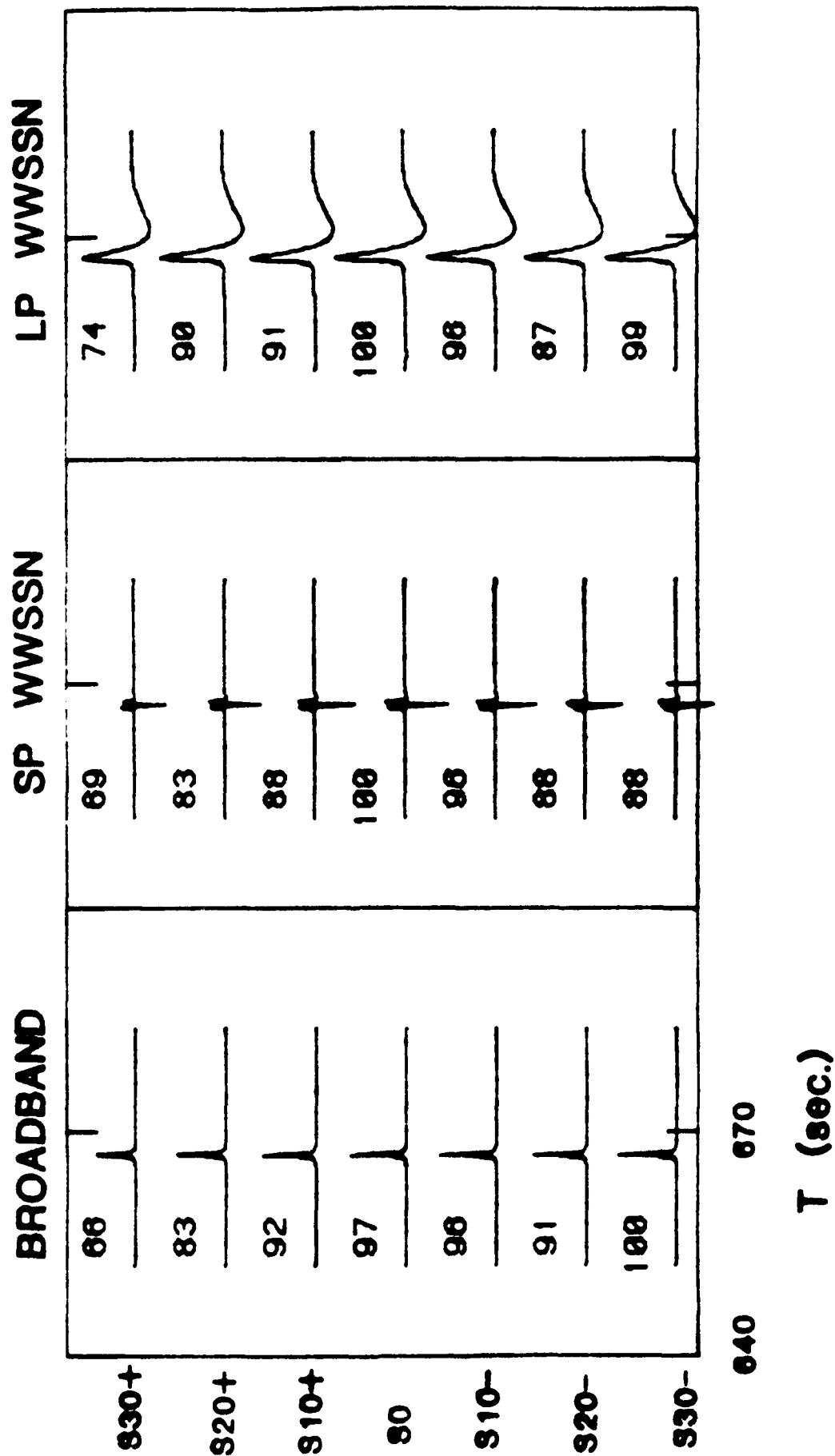the frequency band of observation. This result has important consequences for the

Figure 10. Synthetic seismograms at 70° distance and fixed azimuth for sources at 9.6 km depth and epicentral locations shown in Figure 8.

yield estimation of underground nuclear explosions by measurements of classical body wave magnitudes, m_b, versus broader band measurements of radiated energy in the time and frequency domain. If deep seated, broad scale length (50km and greater), velocity anomalies of 2% or more are a common occurrence in the upper mantle of the earth, they will act to focus and defocus body waves over a broad frequency band. The focussing and defocussing caused by these broad anomalies will be independent of frequency and will thus introduce a scatter in broader band measures of radiated energy which will be equivalent to that seen in the narrow band m_b measurement. Focussing and defocussing by structure in the source region will also affect the coda of P waves if a portion of this coda is generated in the receiver region. These effects may help explain why broader band and integrated coda measures of body wave energy often do not exhibit any less scatter than classical m_b measurements. The broadband and coda magnitudes that exhibit the least scatter typically have 0.15 to 0.2 standard deviation in units of logarithm of energy flux rate over source or receiver arrays having apertures of 200 km (Bullitt and Cormier, 1984). This corresponds to about a 1.5 to 2 variation in the amplitudes of particle velocity, similar to that seen in the synthetic seismograms of Figures 9 and 10. These results suggest that knowledge of the broader scale length velocity anomalies beneath source and receiver sites may be useful in correcting and reducing the scatter in magnitude estimates and hence the uncertainty in yield estimates of nuclear tests.

The frequency independence of the amplitudes calculated in the Zandt model is a characteristic of ray-theoretically predicted amplitudes. It suggests that the Gaussian beam synthesis should not be necessary to accurately calculate amplitude variations due to this receiver structure. There are no caustics in this example and there is no particular advantage to using Gaussian beam superposition over asymptotic ray theory, other than exploiting the paraxial estimation of travel time. Additional evidence of why beam superposition in this example reproduces simple ray theory is illustrated in Figure 11. Ray densities (Figure 11) within the vicinity of a receiver can accurately
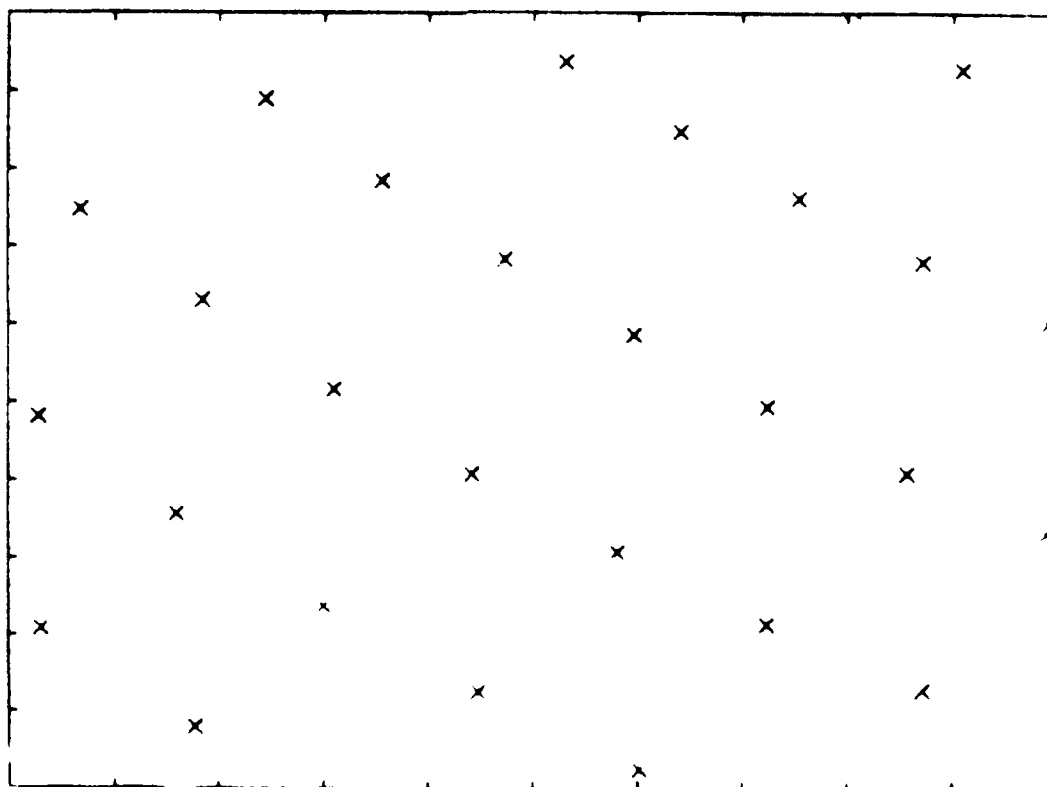
LARGE AMPLITUDE STATION
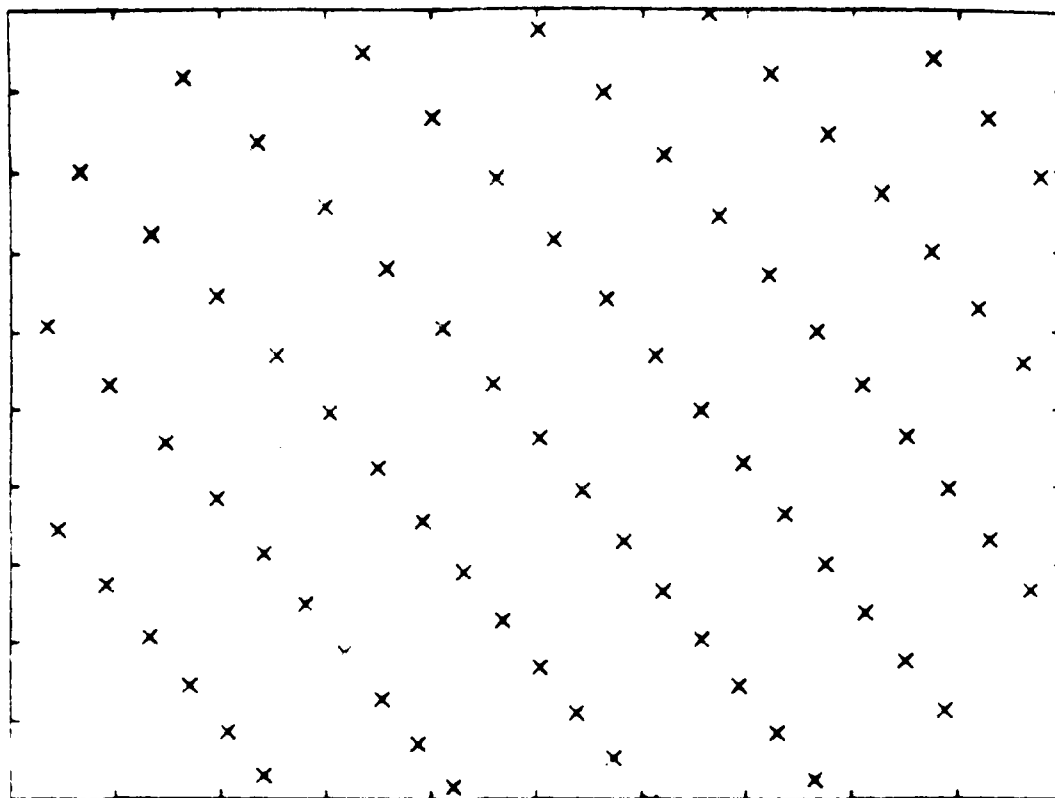
SMALL AMPLITUDE STATION

Figure 11. The end points of rays at the surface of the earth at 70° at high and low amplitude stations in the experiments shown in Figures 9 and 10.

predict the amplitude observed at that receiver. Amplitude is nearly proportional to 1 over the square root of beam density, consistent with the calculation of the geometric spreading by ray tube area.

All combinations of sources and receivers produce ray densities that are similar in form to Figure 11, i.e., uniform over broad regions surrounding each receiver, with no evidence of multipathing. This result is identical to that obtained by Cormier and Aki (1982). They found that multipaths are not generated even when the intensity of anomalies in the Zandt model are doubled. Multipathing, however, depends on the scale length of anomalies as well as intensity. This is emphasized by the results obtained with the second model investigated.

3.2 A RANDOM MODEL

The second model was one generated by perturbing a 1-D model at 10 to 20 km grid points in horizontal planes with an rms velocity fluctuation of 0.8% (McLaughlin and Anderson, 1985). Unlike the Zandt model, this model introduced caustics and multipaths at teleseismic range. This made it essential to use Gaussian beams rather than asymptotic ray theory (ART) to synthesize seismograms at receivers in the vicinity of caustics. ART evaluates the superposition integral by a stationary or saddle point approximation. The stationary phases occur at the discrete rays that solve the two point ray tracing problem between source and receiver, leading to amplitudes proportional to factor $\frac{1}{\sqrt{\det \mathbf{Q}^R}}$. This factor approaches infinity near the caustic surfaces defined by $\det \mathbf{Q}^R = 0$. The superposition integral and its integrand, however, remain regular at caustics for a generalized, complex $\mathbf{M}$ matrix (Červený et al., 1982; Červený, 1985a,b).

3.2.1 Effect of varying source location at constant azimuth

Figure 12 shows contours of velocity at the bottom of the random model and the location of sources in a variable source experiment. The velocity contours have been left unlabled and are shown only to illustrate the dramatically different scale lengths of velocity fluctuation in this model compared to the Zandt model. At a constant azimuth, the amplitude fluctuations (Figure 13) due to variations in source location are both larger and occur more rapidly than those seen in the Zandt model (Figure 10). This reflects the fact that the smallest scale length of velocity fluctuation (10 km.) roughly equals the spacing of source points. Greater frequency dependence of the amplitudes is also seen. This is due, in part, to the presence of caustics in the vicinity of the receivers for some of the source-receiver paths. Figure 14 is a plot of ray end points, illustrating the development of one of these caustics in the vicinity of the 70° station for a source at location s10-. A triplicated zone of end points can be seen, which is elongated along a narrow azimuthal zone. Rays having end points within this zone are found to have a one unit advance in their KMAH index (Ziolkowski and Deschamps, 1980), indicating that these rays have passed through a caustic once. A receiver located within this zone of triplicated end points is likely to observe some phase distortion in its waveform because some of the beams that contribute to the superposition integral will have a $-\frac{\pi}{2}$ phase shift. This phase distortion is difficult to observe in synthetics calculated for a profile of stations r400- to r400+ shown in Figure 15. The phase distortion appears as small change in the rise time of the broadband pulse at station r0. The small negative first break, best visible on the broadband pulse at r0, is not due to the phase shifted beams, but rather due to the unique interference effects of this particular beam pattern. The largest effects to be observed on waveforms might be expected on the short period instrument. The highest frequency band would have the highest per cent contribution from beams within the triplicated region at r0 because beams more distant from r0 would suffer a stronger exponential decay. No substantial modifications, however, are seen in the short period waveform of station r0
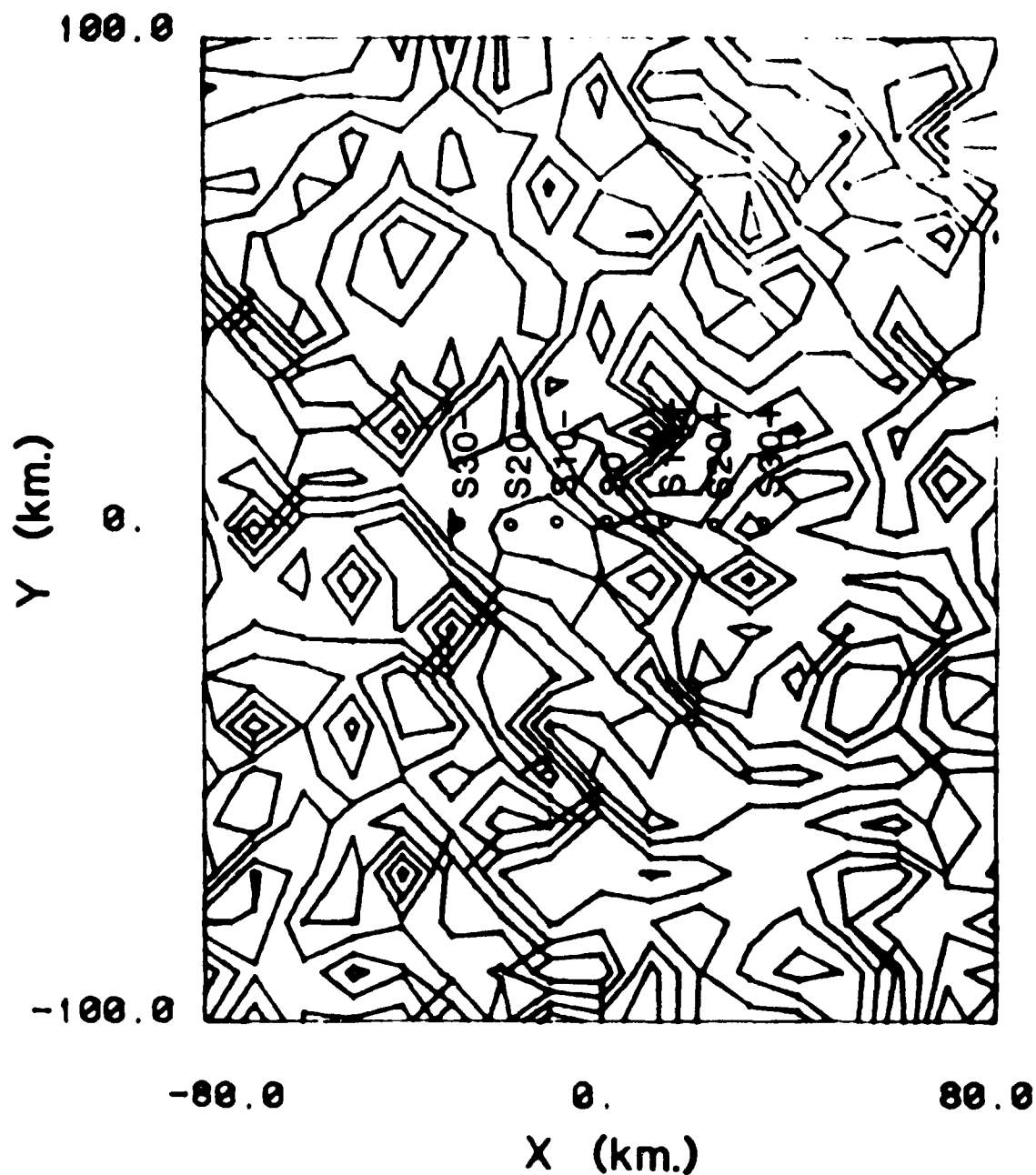
Figure 12 P velocity contours in a horizontal plane at the bottom of a model constructed by adding a 0.8% random perturbation to the velocities of a 1-D model. Perturbations were assigned at 10 to 20 km. spaced grid points the horizontal plane. The contour interval is 0.05 km./sec, which is the same as that shown in Figure 8. The epicentral location of sources s10. to s30+ at 9.6 km. depth are projected onto this plane

BROADBAND
SP WWSSN
LP WWSSN
S 30+
S 20+
S 10+
S 0
S 10-
S 20-
S 30-
53
100
61
37
69
27
37
46
100
66
37
66
27
42
58
100
67
44
74
29
44
640
670
T (SEC.)
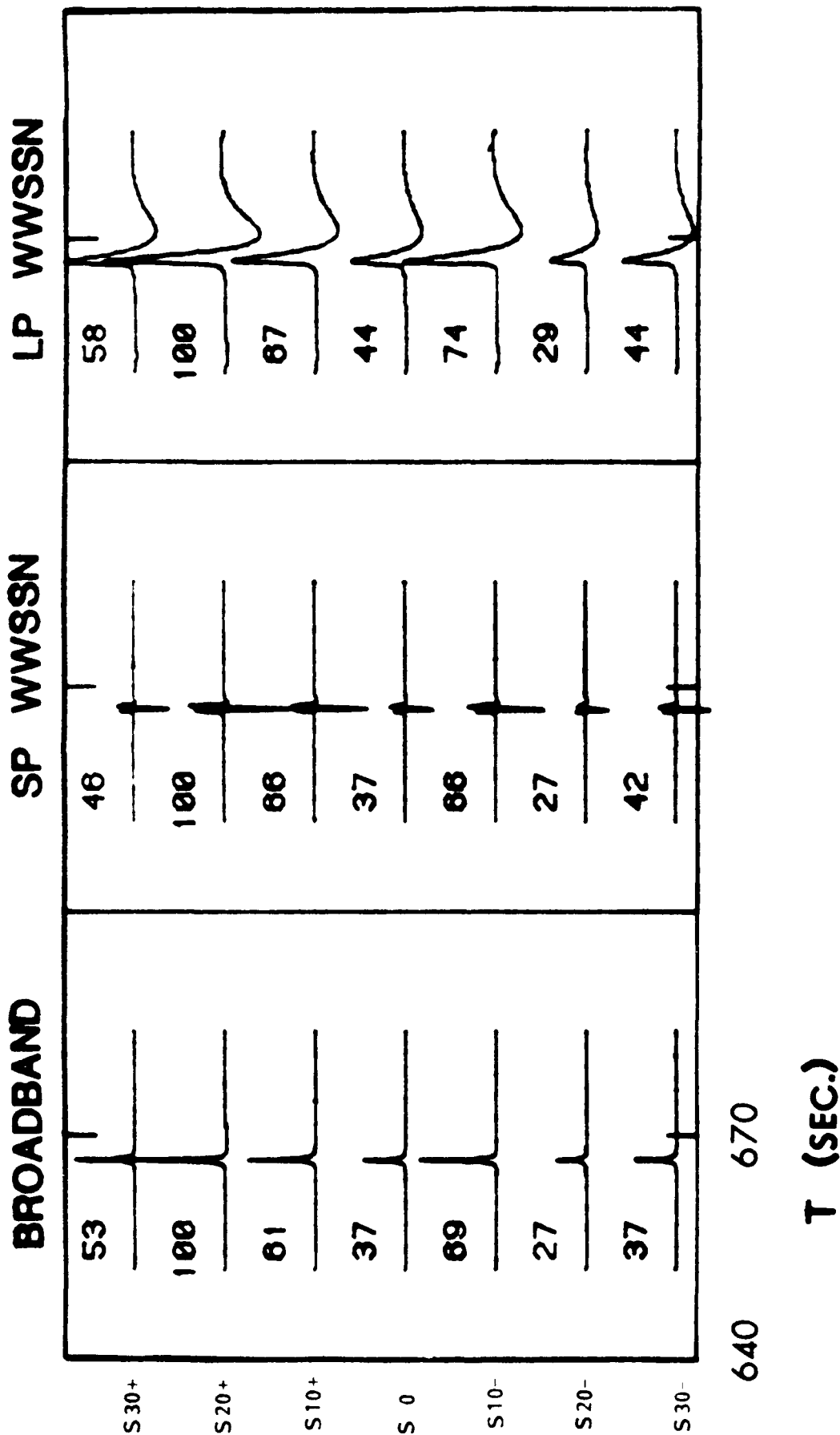
Figure 13. Broad band, short period, and long period synthetic P waves at 70° distance for the sources and random model shown in Figure 12. Azimuth of the station was held constant.
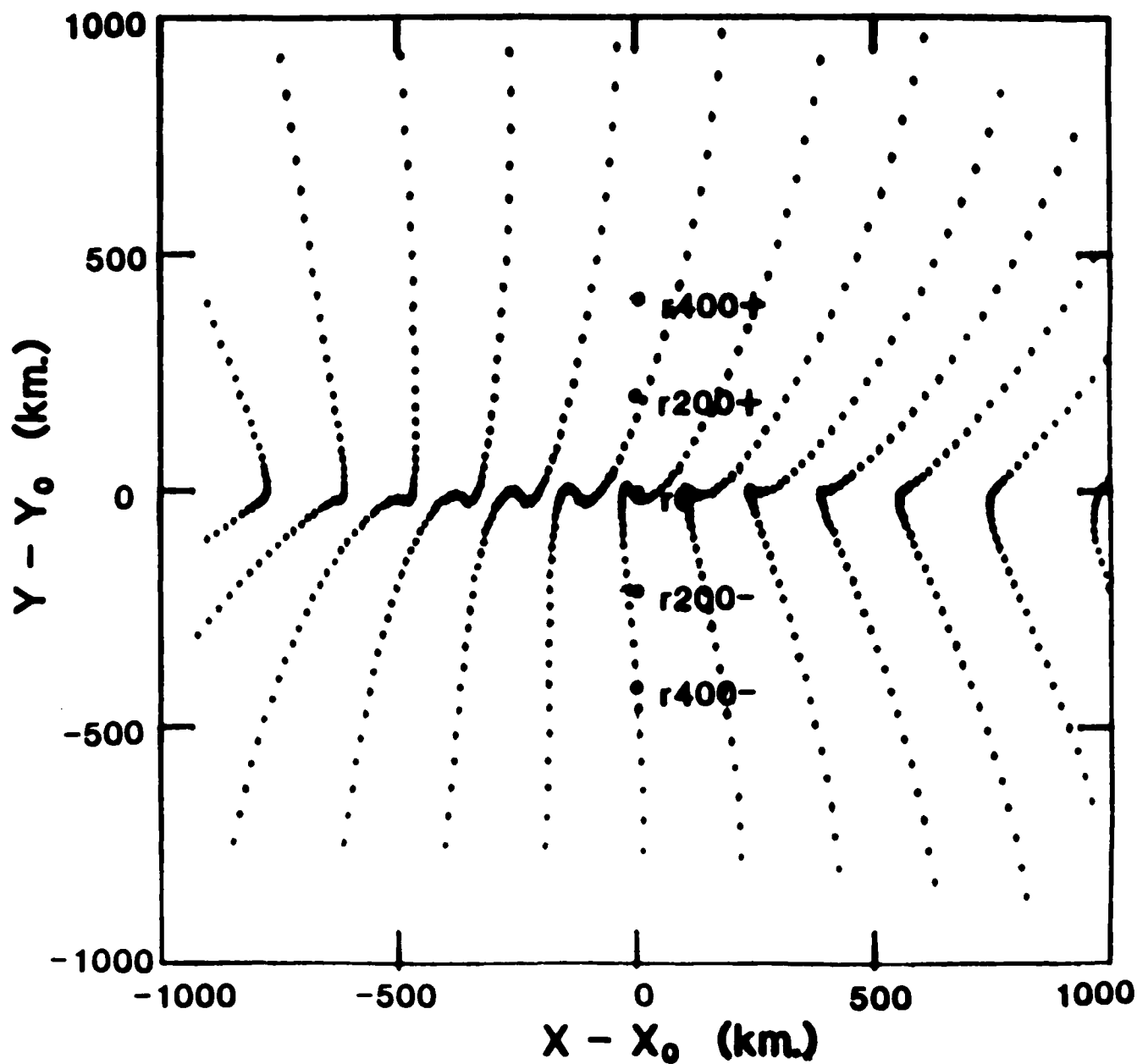
Figure 14. Ray end points near a station at 70° distance from source s10- in the random model. The locations of a profile of stations in the vicinity of a caustic intersection is given by the labled points r400- to r400+.

Figure 15. Synthetic P waves for the profile of stations in the vicinity of the caustic shown in the plot of ray end points in Figure 14.

Comparison of amplitudes in different frequency bands in Figure 15 now shows substantial frequency dependent effects. Long period amplitudes vary only about half as much as short period and broad band amplitudes. A much broader area of beams contribute to the long period response, smoothing over the effect of the caustic region near station r0.

3.2.2 The features that generate caustics and multipaths

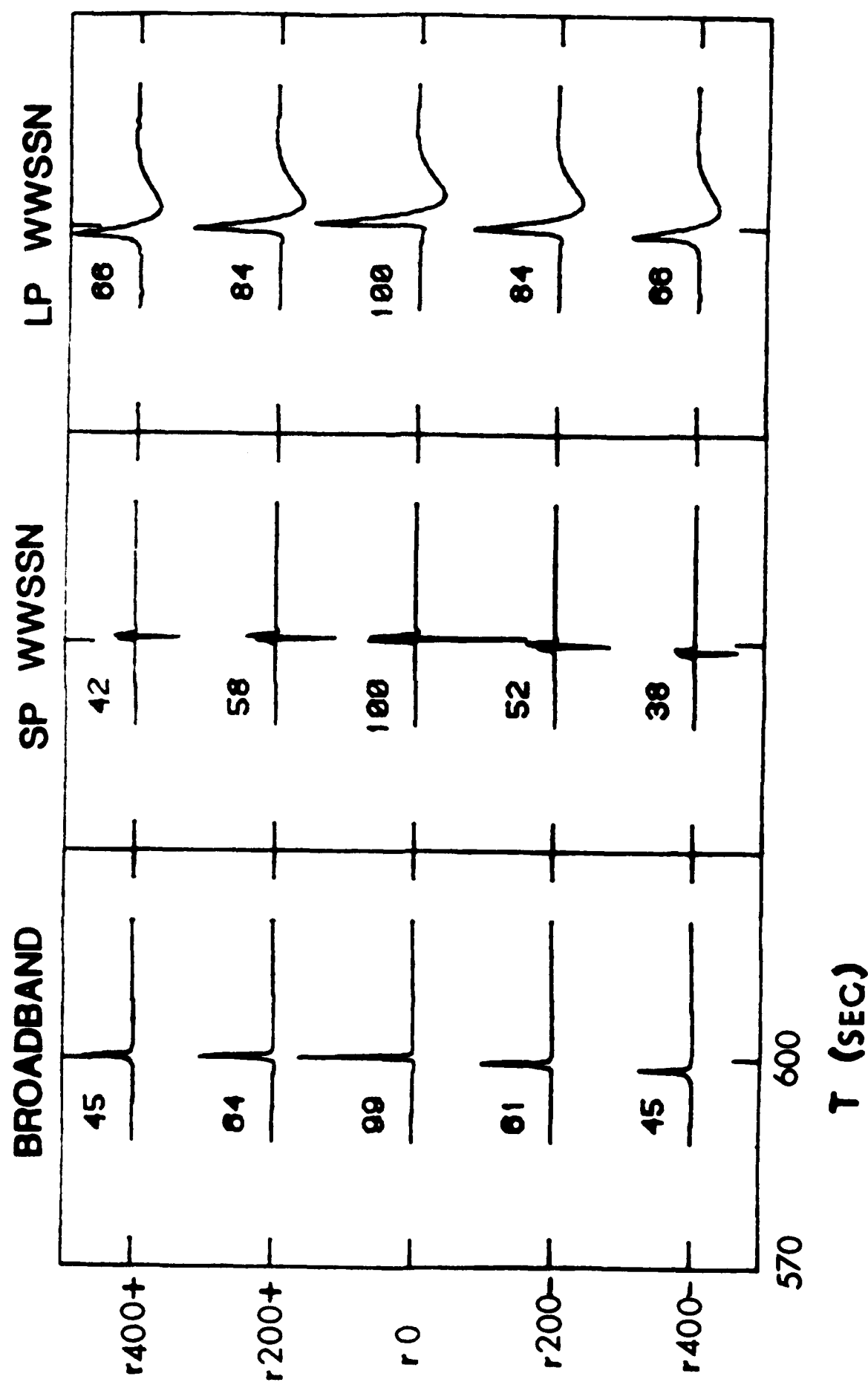Exactly what feature of the random model was responsible for the thin, elongated caustic intersection shown in Figure 14 ? Since this feature is elongated along a particular azimuth, the lateral location of the structure is constrained to be along the ray paths that leave the 3-D portion of the model at this azimuth. The range of vertical take-off angles along this azimuth is also bounded by the apparent edges of the caustic intersections in the plot of ray end points. The calculation of the KMAH index can also be used to identify the particular rays that are tangent to the caustic surface at depth. By either of these methods, the rays that describe the caustic can be identified and their trajectories plotted through the 3-D region of the model. When this is done (Figure 16), it can be seen that the structure responsible for the caustic at teleseismic distance is a low velocity zone, extended in the vertical direction. The reason why such structures have been generated in this random model is that the grid spacing at which velocities were assigned was much larger in the vertical direction (30 km) than in the horizontal direction (10 or 20 km). Thus, there will occasionally be regions of the model where negative perturbations strongly correlate between adjacent vertical grid lines, forming a vertically, elongated zone of low velocities. Similarly, elongated zones of high velocities will be formed. The surprising observation seen with this particular model is that only a very small perturbation of velocity (0.8%), with a vertical scale of 30 to 60 km, and a horizontal scale of 10 km, can generate caustics and phase advances at teleseismic distances. These caustics intersect the surface of the earth at
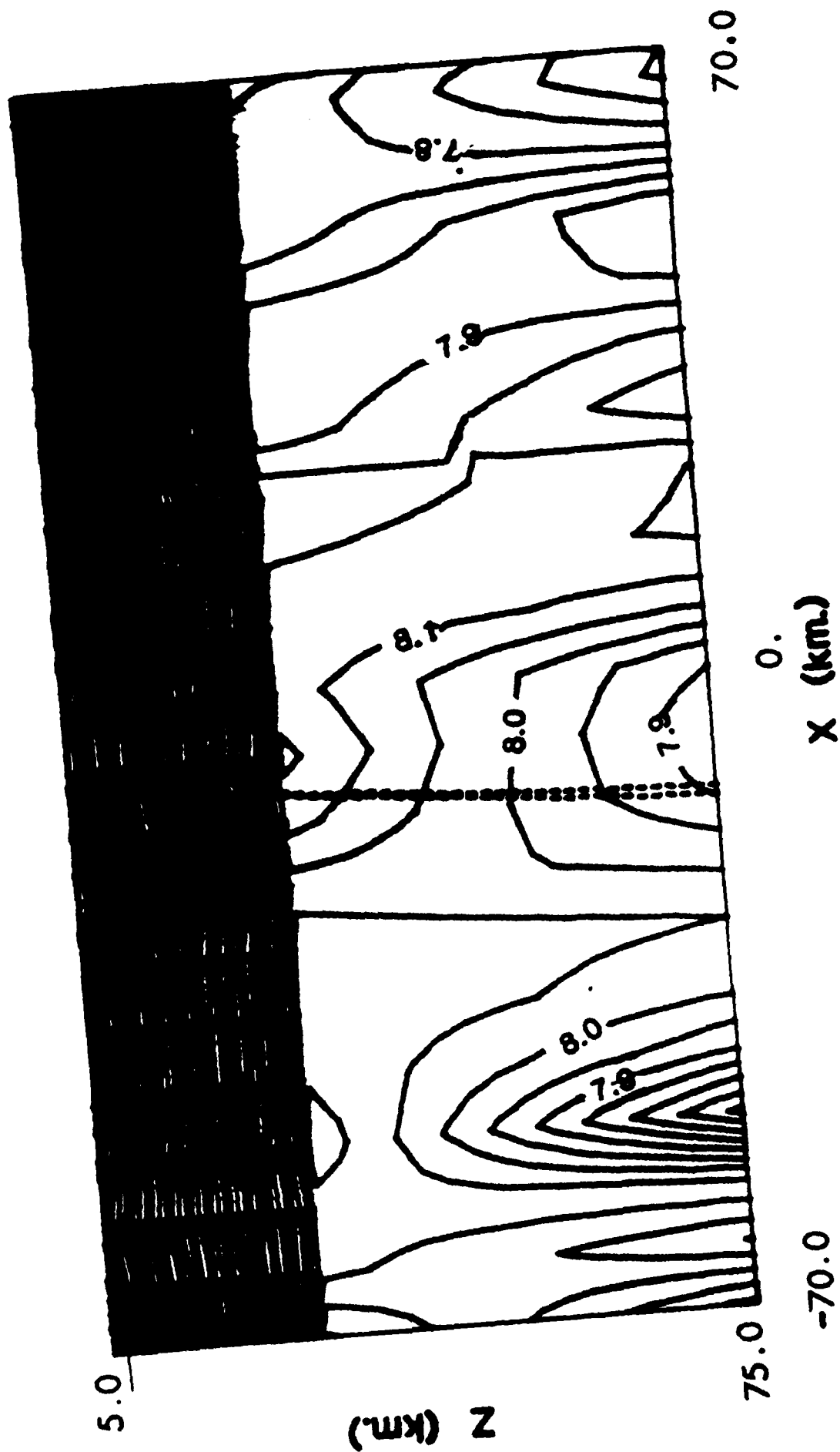
Figure 16. Trajectory of rays in the vicinity of station r0 plotted in the source region. Trajectories are projected onto a plane defined by the location of the source, receiver, and center of the earth. The two rays shown are rays that were shot at constant azimuth and bound a caustic surface formed at teleseismic range. Contours of velocities are shown at a 0.05 km/sec interval.

teleseismic range, but the areal extent of these intersections are too small to be visibly identified except for some rather subtle effects in the waveforms at a few number of stations. The generation of these caustics depends on the strength of velocity fluctuation as well as on the relation between the characteristic vertical and horizontal scale lengths of the 3-D model. In the example considered, the shortest scale length in the vertical direction exceeds that in the horizontal direction, a situation which is probably not the common state of crust/lithospheric structure (McLaughlin, personal communication). Some notable exceptions to this would include regions having concentrations of intrusive pipes and plumes. The results of the single modeling experiment described here suggest that some distributions of heterogeneity would produce unacceptably large effects on teleseismic waveforms. It is clear that forward modeling of the effects of very general distributions of heterogeneities will be useful in defining the "heterospectrum" of the lithosphere. (The heterospectrum is a term adopted by Wu [1986] to embrace both the the strength of velocity fluctuation and its three-dimensional spatial spectrum).

4 Validity of the results

All the example seismograms were calculated by superposition of Gaussian beams. The accuracy of this technique depends both on the validity of using the first term in an asymptotic solution to the elastodynamic wave equation and making a Taylor expansion of the complex phase about the central ray (the paraxial approximation). It is thus appropriate to question whether the 3-D models of velocity discussed in this paper have exceeded the domains of validity of these approximations. Validity constraints in continuous media have been formulated by Beydoun and Ben-Menahem (1985) and Červený (1985b). White et al (1986) have considered problems encountered with continuous media as well with boundary interactions. The simplest constraints to check are those related to the asymptotic expansion, which assumes decoupling of P

and S waves to zeroth order and neglect reflections and conversions by regions of strong gradient. These constraints require that wavelength be much less than quantities such as $\frac{v}{\nabla v}$ and $\frac{\rho}{\nabla \rho}$ (Kravtsov and Orlov, 1980; Beydoun and Ben-Menahem, 1985), where v and ρ are velocity and density respectively. Both the Zandt model and the random model satisfy this constraint throughout the frequency band 0.03 to 4 Hz.

Constraints on the validity of the paraxial approximation and the beam superposition have been cast in terms of the real and imaginary parts of the **M** matrix and distance from the central ray (Beydoun and Ben-Menahem, 1985; Červený, 1985b). In order to see if these constraints are obeyed everywhere along a beam, the **M** matrix must be known everywhere along the central ray associated with that beam. At any point S along the central ray, $\mathbf{M}(S)$ can be found by using the Π matrix to back propagate the complex $\mathbf{M}(Q_s)$ matrix selected at the end point Q_s. Although these constraints were not calculated in the two examples described, a check on the overall validity of the beam superposition was taken from the results of reciprocal experiments, in which the positions of sources and receivers were reversed. Examples of this test in 2-D media are given by Nowack and Aki (1984) and Müller (1984). Reciprocal experiments were conducted in the form of allowing a plane wave to be vertically incident on the 3-D models. The plane wave was expanded into Gaussian beams by the procedure described by Červený (1982), and the wavefield was calculated at receivers on the surface of the 3-D models. Such an experiment was conducted on the random model (McLaughlin and Anderson, 1985) and on a model having a heterospectrum similar in scale length and velocity fluctuation to the Zandt model (Nowack and Cormier, 1985). Although the geometry was not precisely reciprocal and waveforms were not directly compared, both experiments produced intensities and coherence of amplitude fluctuations similar to those produced by the teleseismic experiments.

5 Conclusions

The theory and examples discussed in this paper have shown how the propagator matrix of the dynamic ray tracing equations, Π, can be exploited to connect 3-D to 1-D portions of a model. Both plane wave and point source initial conditions are required to specify the elements of the propagator matrix. Thus, both plane wave and point source solutions are generally useful for all asymptotic methods of body wave synthesis and not just for Gaussian beams.

An investigation was made of the effect of 3-D structure in the source region on the focussing and defocussing of teleseismic P waves. These effects were observed with two different models as a function of source location within the 3-D model and of azimuth at the source. In a 3-D model, block inverted from teleseismic travel times, ray theoretical amplitudes matched those predicted from superposition of Gaussian beams. In this model, the characteristic scale lengths of the most intense velocity fluctuations (4%) were on the order of 50-100 km in the source region. This model produced a factor of two fluctuation in amplitude, associated with fluctuations in travel time on the order of several tenths of a second. Amplitude variations due to variations in source location were small over location variations that were small with respect to the scale length of velocity fluctuation. All amplitude variations were nearly independent of frequency across the body wave band of 0.03 to 4 Hz. The frequency independence of amplitude variations across the body wave band may have important implications for removing the effects of azimuthal amplitude variations due to 3-D structure beneath nuclear test sites. Broad scale length, deep seated structure can affect short period as well as broad band and coda measures of radiated seismic energy. Its effects, however, may be easily correctable if a 3-D model of the source region is known from block inversion of travel time residuals. A resolvable block size of about 20 km may be all that is necessary to formulate corrections based on azimuth of teleseismic station and source location within a test site.

Calculations with a random velocity model demonstrated that a smaller intensity of velocity fluctuation (0.8%) can produce even larger amplitude variations if the smallest scale length of fluctuation is on the order of 10 km. The random model was constructed such that the smallest scale length of velocity fluctuation was shorter in the horizontal direction than in the vertical direction. At teleseismic range, this model generated isolated caustics, which were elongated along the azimuth of approach. The waveform distortion associated with these caustics was small. The fact that the caustics were generated at all by such mild 3-D perturbations is significant. It suggests that this type of synthetic modeling may be useful in limiting some of the attributes of the heterospectrum of the earth's lithosphere.

Acknowledgements

Keith McLaughlin generated the random 3-D models and provided insightful comments on the results of the waveform calculations.

References

Aki, K., Christoffersson, A., and Husebye, E.S., 1976. Determination of three-dimensional seismic structures of the lithosphere, *J. Geophys. Res.*, *82*, 277-296.

Berteussen, K.A., 1975. P wave amplitude variability at NORSAR, *J. Geophys.*, *41*, 595-613.

Berteussen, K.A., A. Christoffersson, E.S. Husebye and A. Dahle, 1975. Wave scattering theory in analysis of P-wave anomalies at NORSAR and LASA, *Geophys. J.R. astr. Soc.*, *42*, 403-417.

Beydoun, W.B., and Ben-Menahem, A., 1985. Range of validity of seismic ray and beam methods in general inhomogeneous media -- I. and II. *Geophys. J. R. astr. Soc.*, *82*, 207-262.

Bullitt, J.T., and Cormier, V.F., 1984. The relative performance of m_b and alternative measures of elastic energy in estimating source size and explosion yield. *Bull Seism. Soc. Am.*, *74*, 1863-1882.

Červený, V., Popov, M.M., and Pšenčik, I., 1982. Computation of wavefields in inhomogeneous media - Gaussian beam approach. *Geophys. J. R. astr. Soc.*, *70*, 102-128.

Červený, V., 1982. Expansion of a plane wave into Gaussian beams, *Stud. Geophys. Geod.*, *26*, 120-131.

Červený, V., and Janský, J., 1983. Ray amplitudes of seismic body waves in inhomogeneous, radially symmetric media, *Stud. Geophys. Geod.*, *27*, 9-18.

Červený, V., L. Klimeš and I. Psencik, 1984. Paraxial ray approximations in the computation of seismic wavefield in inhomogeneous media, *Geophys. J.R. astr. Soc.*, *79*, 89-104.

Červený, V., 1985a. The application of ray tracing to the propagation of shear waves in complex media, in *Seismic Exploration*, eds. Treitel, S., and Helbig, K., Vol. on Seismic Shear Waves, ed. Dohr., G., Geophysical Press, pp. 1-124.

Červený, V., 1985b. Gaussian beam synthetic seismograms, *J. Geophys.*, *58*, 44-72.

Comer, R. and Aki, K.,1982. Effects of lateral heterogeneity near an earthquake source on teleseismic raypaths, *Earthquake Notes*, *52*, no. 1.

Cormier, V.F., 1986. An application of the propagator matrix of dynamic ray tracing: the focussing and defocussing of body waves by three-dimensional velocity structure in the source region, *Geophys. J. R. Astr. Soc.*, submitted.

Dziewonski, A.M., and Anderson, D.L., 1981. Preliminary reference earth model (PREM). *Phys. Earth Planet. Inter.*, *25*, 297-356.

Haddon, R.A.W. and E.S. Husebye, 1978. Joint interpretation of P-wave time and amplitude anomalies in terms of lithospheric heterogeneities, *Geophys. J.R. astr. Soc.*, *55*, 19-43.

Haines, A.J., 1983. A Phase Front Method - I. Narrow frequency SH waves, *Geophys. J R*

astr Soc., *72*, 783-808.

Haines, A.J. and C.J. Thomson, 1986. Comparison of P-wave amplitude from ray tracing and the phase-front parabolic approximation for a three-dimensional structure, submitted to *Geophys J R astr Soc*

Klimes, L., 1984. Expansion of a high-frequency time-harmonic wavefield given on an initial surface into Gaussian beams, *Geophys. J R. astr Co.*, *79*, 105-118.

Kravtsov, Y.A., and Orlov, Y.I., 1980. Limits on the applicability of the method of geometric optics and related problems, Sov. Phys. Usp., 23, 750-762.

Madariaga, R., and Papadimitriou, P., 1985. Gaussian beam modelling of upper mantle phases, *Ann Geophys*, *3*

McLaughlin, K.L., and L.M. Anderson, 1985. Stochastic dispersion of P waves due to scattering and multipathing, Teledyne-Geotech, Final Report No. TGAL-85-8, ARPA Order No. 4511.

Minster, J.B., Savino, J.B., Rodi, W.L., Jordan, T.H., and Masso, J.F., Three-dimensional velocity structure of the crust and upper mantle beneath the Nevada Test Site, SSS-R-81-5138, S-Cubed, La Jolla, California, 1981.

Müller, G., 1971. Approximate treatment of elastic body waves in media with spherical symmetry, *Geophys J*, *23*, 435-449.

Nowack, R. and Aki, K., 1984. The 2-D Gaussian beam method: testing and application, *J Geophys Res*, *89*, 7797-7819.

Nowack, R.L., and Cormier, V.F., 1985. Computed amplitudes using ray and beam methods for known 3-D structures (abstract), *EOS, Trans Am Geophys Un.*, *66*, 980.

Thomson, C.J. and D. Gubbins, 1982, Three-dimensional lithospheric modeling at NORSAR: Linearity of the method and amplitude variations from the anomalies, *Geophys J R astr Soc*, *71*, 1-36.

Thomson, C.J., 1983. Ray-theoretical amplitude inversion for laterally varying structure below NORSAR, *Geophys J R astr Soc*, *74*, 525-558.

Thomson, C.J. and C.H. Chapman, 1985. An introduction to Maslov's method, *Geophys J R astr Soc*, *83*, 143-168

White, B.S., Burridge, R., Noriss, A., and Bayliss, A., 1986. Some remarks on the Gaussian beam summation method, Geophys. J. R. Astr. Soc., submitted.

Wu, R-S., 1986. Heterogeneity spectrum, wave scattering response of a fractal medium and the rupture processes in the medium, *J of Wave-Material Interaction*, submitted.

Zandt, G., 1981. Seismic images of the deep structure of the San Andreas Fault system, central coast ranges, California, *J Geophys Res*, *86*, 5039-5052.

Ziolkowski, R.W., and Deschamps, G.A., 1980. The Maslov method and the asymptotic

Fourier transform: caustic analysis, Electromagnetics Laboratory Scientific Report No. 80-9, University of Illinois at Urbana-Champaign.

END
DTIC
9-86